

Observations on spatial variations of the Sr I 4607 Å scattering polarization signals at different limb distances with ZIMPOL

Sajal Kumar Dhara¹, Emilia Capozzi¹, Daniel Gisler^{1,2}, Michele Bianda¹, Renzo Ramelli¹, Svetlana Berdyugina², Ernest Alsina¹, and Luca Belluzzi¹

¹ Istituto Ricerche Solari Locarno (IRSOL), 6605 Locarno-Monti, Switzerland,
e-mail: sajal@irsol.ch

² Kiepenheuer-Institut für Sonnenphysik (KIS), Schöneckstrasse 6, 79104 Freiburg, Germany

August 12, 2019

ABSTRACT

Context. The Sr I 4607 Å spectral line shows one of the strongest scattering polarization signals in the visible solar spectrum. The amplitude of this polarization signal is expected to vary at granular spatial scales, due to the combined action of the Hanle effect and the local anisotropy of the radiation field. Observing these variations would be of great interest because it would provide precious information on the small-scale activity of the solar photosphere. At present, few detections of such spatial variations have been reported. This is due to the difficulty of these measurements, which require combining high spatial ($\sim 0.1''$), spectral (≤ 20 mÅ), and temporal resolution (< 1 min) with increased polarimetric sensitivity ($\sim 10^{-4}$).

Aims. We aim to detect spatial variations at granular scales of the scattering polarization peak of the Sr I 4607 Å line at different limb distances, and to study the correlation with the continuum intensity.

Methods. Using the Zürich IMaging POLarimeter (ZIMPOL) system mounted at the GREGOR telescope and spectrograph in Tenerife, Spain, we carried out spectro-polarimetric measurements to obtain the four Stokes parameters in the Sr I line at different limb distances, from $\mu = 0.2$ to $\mu = 0.8$, on the solar disk.

Results. Spatial variations of the scattering polarization signal in the Sr I 4607 Å line, with a spatial resolution of about $0.66''$, are clearly observed at every μ . The spatial scale of these variations is comparable to the granular size. A statistical analysis reveals that the linear scattering polarization amplitude in this Sr I spectral line is positively correlated with the intensity in the continuum, corresponding to the granules, at every μ .

Key words. Sun: photosphere, Sun: granulation, Polarization, Scattering, Instrumentation: high angular resolution, Magnetic field

1. Introduction

The Sr I 4607 Å photospheric line shows one of the strongest scattering polarization signals (above 1% at $\mu = \cos(\theta) = 0.1$, where θ is the heliocentric angle; see e.g., Stenflo et al. 1997; Gandorfer 2002) in the visible solar spectrum. This signal is sensitive to the Hanle effect and can be used as an excellent diagnostic tool for investigating weak turbulent magnetic fields in quiet photospheric regions (Faurobert-Scholl 1993; Faurobert et al. 2001). By solving the radiative transfer problem of scattering line polarization in a realistic three-dimensional (3D) hydrodynamical model of the solar photosphere, Trujillo Bueno & Shchukina (2007) foresee appreciable small-scale spatial variations of the amplitude of the scattering polarization signals in the Sr I 4607 Å line, provided that granulation is resolved. The origin of such variations is related to variations in the magnetic field present in the granules or the intergranular lanes, and to the local variations in the anisotropy of the radiation field. Unfortunately, detecting these spatial variations is challenging. Observations with the polarimetric sensitivity required to detect this scattering polarization signal, generally suffer from insufficient spatial and temporal resolution (Trujillo Bueno & Shchukina 2007). A further difficulty is due to the fact that scattering polarization signals decrease when moving from the solar limb to the disk center, while the granulation

can be clearly resolved only if the observed region is sufficiently far from the limb.

Malherbe et al. (2007) performed spectro-polarimetric observations of the Sr I 4607 Å line at $40''$ ($\mu \sim 0.3$) inside the solar limb with a spatial resolution of about $0.6''$. Their observations reported that intergranules are generally less polarized than the granules, thus suggesting stronger magnetic fields in the intergranular lanes. Their findings perhaps hint at a Hanle effect acting in the intergranules (meaning in higher magnetic field regions), in agreement with simulations carried out by Trujillo Bueno et al. (2004). Bianda et al. (2018) carried out spectro-polarimetric observations at $\mu = 0.3$ close to the east limb using the Zürich IMaging POLarimeter (ZIMPOL: Ramelli et al. 2010) at the GREGOR telescope (Schmidt et al. 2012; Ramelli et al. 2014). Their observations also revealed small-scale spatial variation of the scattering polarization signal of the Sr I 4607 Å line, and confirmed that the amplitudes are generally higher at the center of the granules than in the intergranular lanes, meaning the polarization signal is positively correlated to the continuum intensity.

Recently, del Pino Alemán et al. (2018) performed 3D radiative transfer calculations in a high-resolution magneto-convection model, finding an anticorrelation between the amplitude of the theoretical scattering polarization signal of the

Sr I 4607 Å line and the continuum intensity at all on-disk positions. Their work also shows how the predicted amplitudes and spatial variations are modified after degrading the signal-to-noise ratio (S/N) and the spectral and spatial resolutions of the simulated observations. Stokes filtergraph observations of the Sr I 4607 Å line have been carried out by Zeuner et al. (2018) with the Fast Solar Polarimeter (FSP; Feller et al. 2014; Iglesias et al. 2016) mounted on Telecentric Etalon Solar Spectrometer (TESOS) at the German Vacuum Tower Telescope (VTT; Soltau 1981), Tenerife, Spain. The TESOS Fabry-Perot tunable filtergraph has a full-width at half maximum (FWHM) of about 25 mÅ. These observations performed at $\mu = 0.6$ toward the north solar limb for field of view (FOV) 20"×20", sampled with 0.16" pixel⁻¹. They scanned the Sr I absorption line at five wavelength positions with a step of 30 mÅ and 2.5 s integration time at each position. Their results shows an anti-correlation between the amplitudes of the Stokes Q/I signals and the continuum intensity. The observed larger scattering polarization signals in the intergranules is in qualitative agreement with theoretically predicted by Trujillo Bueno & Shchukina (2007) and del Pino Alemán et al. (2018).

As a further step along this line of research, we carried out an observing campaign during June 2018 at the GREGOR solar telescope in Tenerife, using the ZIMPOL polarimeter system. Our main aim was to measure small-scale spatial variations of the Sr I 4607 Å scattering polarization signal, at different limb distances on the solar disk. We describe the observations with the GREGOR telescope and the data reduction process in Sect. 2. We study the possible presence of correlations between the amplitudes of the scattering polarization signals and the continuum intensity, Sect. 3, which we have used as an indicator of the locations of granules and intergranular lanes, at the various limb distances considered. A discussion of our results is presented in Sect. 4.

2. Observations with GREGOR

Our observational campaign at the GREGOR telescope was held between 13 June 2018 and 27 June 2018. The ZIMPOL system was installed at the GREGOR spectrograph. The polarimeter analyzer consists of a double ferroelectric crystal modulator, followed by a linear polarizer. It was mounted in front of the spectrograph slit. The ferroelectric crystal modulates the signals at the frequency of 1 kHz, thus allowing minimal spurious effects induced by intensity variations due to the seeing. A synchronous demodulation can be obtained with the ZIMPOL camera, which has a masked charge-coupled device sensor equipped with cylindrical microlenses (for details see Ramelli et al. 2010). During our observation we also used the image derotator, which allows to maintain the slit orientation with respect to the rotating solar image. This is thus an advantage for performing long exposure measurements. However, the disadvantage of using the image derotator is that it introduces extra variable instrumental polarization. Thus, more calibrations are needed during the observations. At noon, we did not perform observations as the Sun is near to zenith and the image rotation is rapid ($>80'' \text{ s}^{-1}$). By contrast, it is quite stable ($< 20'' \text{ s}^{-1}$) during the early morning and the evening.

The observations were performed at quiet regions of the Sun, at different limb distances on the solar disk from $\mu=0.2$ to 0.8. The date, limb distances, and other details of the observations are given in Table 1. We used the adaptive optics (AO) system (Berkefeld et al. 2016) for all measurements in order to get sta-

ble observations for the required field-of-view (FOV) positions. Close to the disk center ($\mu = 0.8$ to 0.4), the granular structures were used by the Shack-Hartmann wavefront sensor to lock the AO system; while closer to the limb ($\mu = 0.2$), where the intensity contrast is low, bright plage regions present in the FOV were used instead during observations. The spectrograph slit was almost always placed away from active regions, parallel to the nearest limb. The seeing quality fluctuated during our observations. Observations taken into account in the analysis are only those with a spatial resolution better than 1" for at least ~ 2 min, during which granular and intergranular regions are well distinguished. The observed Fried parameters during our measurements are listed in Table 1. The spectrograph slit covers a solar area of 0.3" (width of the slit) times 47" (length of the slit). The obtained ZIMPOL image has a spatial scale of $\sim 0.33''$ per pixel and it contains 140 pixels in the spatial direction. The estimated spatial resolution of the Stokes images, under adequate seeing conditions, is found to be 0.66", but it changes for different sets of measurements depending upon the seeing conditions. The spectral resolution of our observation is of 10 mÅ. We used the GREGOR polarimetric calibration unit (Hofmann et al. 2012), which is mounted at the second focal point before any folding reflection, in order to avoid any significant instrumental polarization produced by the mirrors.

For all selected regions, we followed an observing procedure similar to the one adopted in the campaign of the previous year, (see Bianda et al. (2018) for further details). In brief, the observing procedure is the following. i) Acquisition of instrumental polarization measurements are used to calculate special ZIMPOL camera timing parameters, which are needed to electronically compensate the large instrumental polarization (see Ramelli et al. 2014, for more details). ii) Polarimetric calibration is performed using the GREGOR polarimetric calibration unit including dark frame measurement. The acquired data are used to calculate the demodulation matrix. iii) Flat fielding was taken by moving the telescope in quiet regions at the solar disk center. iv) Finally, scientific observations were performed in the selected region. The steps (ii) and (iii) are repeated again after the scientific observation. We have taken series of frames at every observed region depending upon the seeing conditions. One single frame contains the four modulated intensities to calculate the four Stokes parameters, but a series of four images are required to eliminate the spurious detector effects (Gisler 2005; Ramelli et al. 2014). A typical exposure time for a single acquisition is 1 s. Therefore, with an additional overhead time, we can only reach a minimum time resolution around 7 s to digitize and transfer data.

3. Data analysis and results

Data collected during the polarization calibration procedure before each measurement was used to generate the calibration matrix, which was subsequently used to calculate the Stokes images acquired with ZIMPOL. Stokes intensity images were corrected for flat field, and taken close to measurement time.

The statistical noise for a single Stokes image is comparable to the amplitude of the signals in the Sr I line. The root mean square (rms) noises are calculated in a continuum area located in the Stokes Q/I image for each measurement. The rms pixel noise obtained from a single frame are shown in Table 2. In order to improve the S/N in the Stokes images, it is necessary to average a set of frames. But, one also needs to continue preserving the spatial and temporal resolutions. The fourth column of Table 2

Table 1. Details of observations performed during campaign. The spectrograph slit was placed parallel to the nearest limb of the Sun during measurements.

Limb distances (μ)	Date of observations	Slit position on the solar disk	Total duration (min)	no. of frames acquired	Fried parameter (r_0) during measurements
0.2	27 June	near W limb	8.9	80	5 cm, a small plage region is used to lock the AO.
0.38	23 June	near E limb, close to sunspot	3.4	30	4 cm.
0.4	16 June	near N limb	16.5	148	5 – 10 cm.
0.44	23 June	near E limb, close to sunspot	6.7	60	4 – 7 cm.
0.5	16 June	near N limb	16.5	148	4 – 7 cm, sometimes AO was unstable.
0.6	27 June	near W limb	8.9	80	4 – 5 cm, sometimes AO was unstable.
0.7	21 June	near N limb	16.5	148	3 – 5 cm, sometimes AO was unstable.
0.8	16 June	near N limb	14	125	5 – 10 cm.
disk center	21 June	–	16.5	148	5 – 7 cm.

Table 2. For each measurement at a different μ , we report the approximate rms pixel noise of a single Stokes Q/I image (second column) as well as of the image obtained after averaging various frames (third column) and the estimated spatial resolution (last column) for a single frame and averaged frame.

Limb distances (μ)	Q/I rms noise (%) (1 frame)	Q/I rms noise (%) (No. of frames averaged, total integration time)	Estimated spatial resolution	
			single frame	averaged frame
0.2	0.92	0.25 (12 frames, 1.34 min)	0.66" - 0.99"	0.66" - 0.99"
0.38	0.72	0.16 (22 frames, 2.46 min)	0.66"	0.66" - 0.99"
0.4	0.73	0.19 (16 frames, 1.78 min)	0.66"	0.99"
0.44	0.69	0.18 (19 frames, 2.12 min)	0.66"	0.66" - 0.99"
0.5	0.76	0.13 (29 frames, 3.24 min)	0.66" - 0.99"	0.66" - 0.99"
0.6	1.00	0.22 (26 frames, 2.90 min)	0.66" - 0.99"	0.66" - 0.99"
0.7	0.72	0.14 (33 frames, 3.68 min)	0.66"	0.66" - 0.99"
0.8	0.82	0.12 (62 frames, 6.98 min)	0.66"	0.66"
disk center	0.73	0.11 (50 frames, 5.58 min)	0.66"	0.66"

shows the number of frames over which we averaged to improve the S/N for the measurements at different limb distances.

Figure 1 shows the Stokes images corresponding to different limb distances between $\mu=0.2$ and $\mu=0.8$, obtained after averaging over sequentially registered frames (see the third column of Table 2 for the corresponding number of frames averaged). In the Stokes I image one can recognize intensity variations along the spatial direction due to the granulation. The Stokes Q/I image shows the scattering polarization peak in the Sr I 4607 Å line. The polarization peak shows clear spatial variations; their detection was indeed the main goal of our observations. In the Stokes U/I image, there is no signal in the Sr I line core. In the Stokes V/I image, one can recognize the typical patterns of the longitudinal Zeeman effect.

3.1. Solar evolution and image accumulation

In order to improve the S/N in the Stokes images, a few subsequent frames were averaged over time. The number of frames considered in the average is selected by verifying through visual inspection that the granular and intergranular regions are well distinguished over time and they have not significantly evolved during the corresponding time interval. We adopted this visual estimation of the solar granulation evolution to choose the appropriate time interval for performing the temporal average. As an example, we consider the observation performed at $\mu=0.4$. The data series contains 148 frames corresponding to a total ob-

serving time of about 16.5 min. Taking into account the lifetime of granulation, we averaged 16 subsequent frames of the time series (integration time of about 1.78 minutes), so as to reach a sufficient S/N. The ensuing Stokes images are shown in Fig. 1 (panel B). To evaluate whether this temporal averaging introduced significant spatial degradation in our data, we generated a space-time map of the frames seen by the spectrograph slit at a continuum wavelength. An example map is shown in Fig. 2 (panel A), where the continuum intensity is presented in gray scale as a function of the spatial position along the slit (x-axis) and time (y-axis). This map shows the evolution of granulation over time. The observed granular structures remain unchanged within several minutes. A single continuum intensity profile is shown as an example in Fig. 2 (panel B). This profile is obtained by averaging over 1.78 minutes (corresponding to 16 frames) from the beginning, and is normalized with respect to the maximum value. The variation of the intensity profile allows to distinguish the granular regions (larger intensity) and intergranular lanes (lower intensity). The final Stokes images are obtained by averaging with a temporal window width of ~ 1.78 minutes (16 frames), shifted in increments of 16 frames (to avoid data overlap). A few frames have been discarded due to poor seeing conditions during our observation. Those frames are easily identified from the space-time map (Fig. 2, panel A) by visual inspection, when granular and intergranular regions are not well defined.

Similar reduction processes have been applied to other sets of data obtained at different μ . The total number of frames ac-

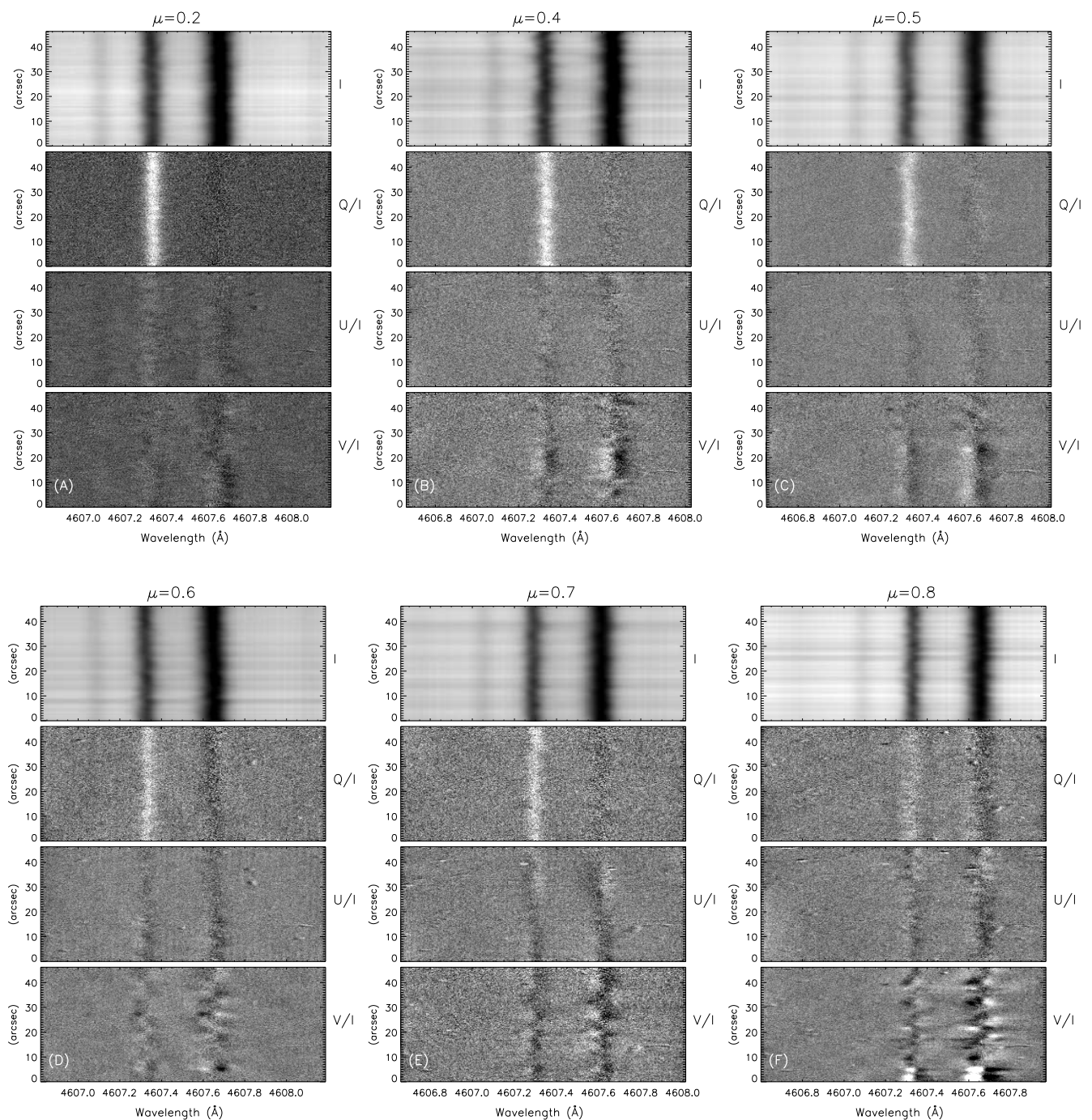


Fig. 1. Stokes images of spectral interval around Sr I 4607 Å line. The spatial direction spans $\sim 47''$ on the solar disk. The observed regions were at different limb distances ($\mu = 0.2, 0.4, 0.5, 0.6, 0.7,$ and 0.8). The slit was placed parallel to the nearest limb. The reference direction for positive Stokes Q is the tangent to the nearest solar limb. These Stokes images are obtained after averaging over several frames (see Table 2). The granulation pattern is visible in the intensity Stoke image, especially in the continuum. The Q/I image shows the scattering polarization peak in the core of the Sr I line. Spatial variations at granular scales of this peak can be observed. The typical antisymmetric Zeeman patterns can be easily recognized in several Stokes V/I images.

quired at every μ is given in Table 1. The number of averaged frames over time (meaning the temporal window width of each data set) is selected following a visual estimation of the solar granulation evolution discussed above, allowing at the same time a good S/N at each μ . These are mentioned in the third column of Table 2. The temporal window width of each data set was chosen by visually inspecting the obtained space-time maps at

every μ . Close to the disk center, between $\mu=0.5$ and 0.8 , the Q/I signal is low, as such, it is necessary to average over a longer time duration in order to sufficiently improve the S/N. While from $\mu=0.4$ to 0.2 , the signal increases as a smaller number of averaged frames are required. The left panel of Fig. 3 shows the space-time map of images seen by the spectrograph slit at the disk center. One can clearly see the evolution of the granulation.

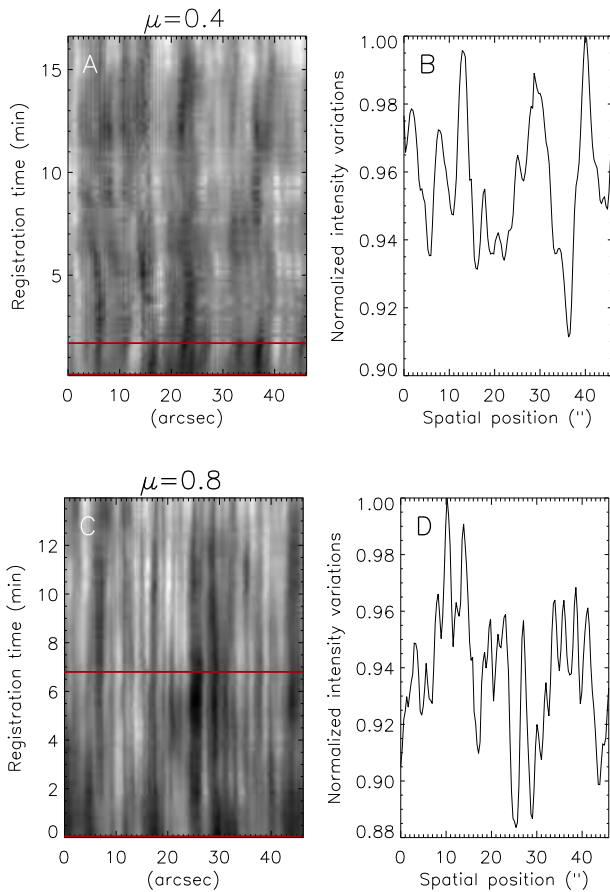


Fig. 2. (A): Space-time map corresponding to observation at $\mu = 0.4$. This map is generated by plotting the continuum intensity profile along the horizontal axis, obtained from each Stokes I images (of 148 total frames) along the spectrograph slit. Each profile was obtained at 6.7 seconds, so that the whole measurement shows a temporal evolution of the FOV of the spectrograph slit of 16.5 minutes. (B): Normalized continuum intensity profile, obtained by averaged over 1.78 minutes from observation beginning. The corresponding time interval is indicated between the red horizontal lines in the space-time map. This profile is used as a parameter to indicate the granular and intergranular regions in Fig. 5. (C): Space-time map corresponding to observation at $\mu=0.8$. (D): Normalized continuum intensity profile. This was obtained by averaging over 6.98 minutes from the beginning of the observation (the corresponding time interval is indicated between red horizontal lines in the space-time map).

Few frames have been discarded for final data reduction due to poor seeing conditions. The right panel of Fig. 3 shows the obtained averaged Stokes images. The Stokes Q/I and U/I images present no signal in the Sr I 4607 Å line.

3.2. Stokes Q/I signal peak

The amplitude of the Q/I signal peak in the Sr I line at every spatial position is calculated using a Gaussian fit to each of the 140 profiles. Figure 4 shows Q/I profiles obtained from a single pixel position (arbitrarily chosen at 9" spatial position) for $\mu = 0.2$ to 0.8, corresponding to the Stokes Q/I images shown in Fig. 1. The red lines are the Gaussian fits to the profiles. We used the GAUSSFIT function available in the interactive data language to fit the Q/I profiles. An estimate of the 1-sigma error of the returned parameters for each fit was also calculated by the fitting

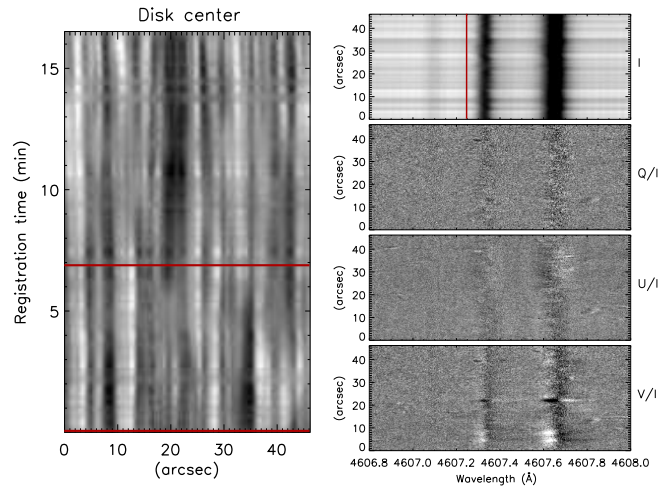


Fig. 3. Left: Space-time map obtained at disk center. Right: Stokes images observed at disk center. These were observed in a spectral interval around the Sr I 4607 Å line, and averaged over ~ 5.58 minutes (50 frames) from the beginning of the observation (see the temporal interval between horizontal red lines in the space-time map). The red vertical line in the Stokes I image shows the wavelength position used to generate the space-time map.

procedure. The fitted amplitudes and error are stored for further investigations. Our obtained Q/I amplitudes are consistent with those obtained by Stenflo et al. (1997). Clear spatial variations of the amplitudes of the Q/I peaks can be appreciated at different μ positions under adequate seeing conditions. Such variations are of solar origin and are no longer detectable when seeing conditions deteriorate give that granular regions and intergranular lanes cannot be easily distinguished.

3.3. Correlations of Q/I with the continuum intensity

The scatter plots shown in Fig. 5 allow us to study the correlations between the polarimetric Q/I peak signals of the Sr I 4607 Å line (y-axis) and the normalized continuum intensity (x-axis), with each panel corresponding to a different μ between 0.2 and 0.8. The continuum intensities are obtained from the space-time maps as described in section 3.1. The error in the Q/I peak amplitudes is estimated from the Gaussian fit procedure applied to the profile. The solid line in the plot is a linear regression (obtained with the linfit function available in the interactive data language). Figure 6 shows the Stokes I, Q/I images and scatter plots measured at the east limb 100" ($\mu=0.44$) and 74" ($\mu=0.38$) inside the solar limb. In the measurements taken at $\mu = 0.44$, part of the slit is over an active region; such spatial positions were excluded (two red horizontal lines showing the excluded spatial portion in the Stokes I and Q images) from the calculation of the correlation coefficient. For all the measurements the obtained slope of the linear regression is positive, suggesting a trend of increasing linear polarization in the higher intensity regions. The Pearson correlation coefficients (r) obtained from each of the scatter plots, are shown both in the plots themselves and in Table 3. The obtained correlation coefficients are positive for all μ . Furthermore, the statistical significance of the obtained coefficients (r) were evaluated by determining the p -values. The p -value is the probability of finding the corresponding r -coefficients provided the null hypothesis (i.e., the lack of correlation between

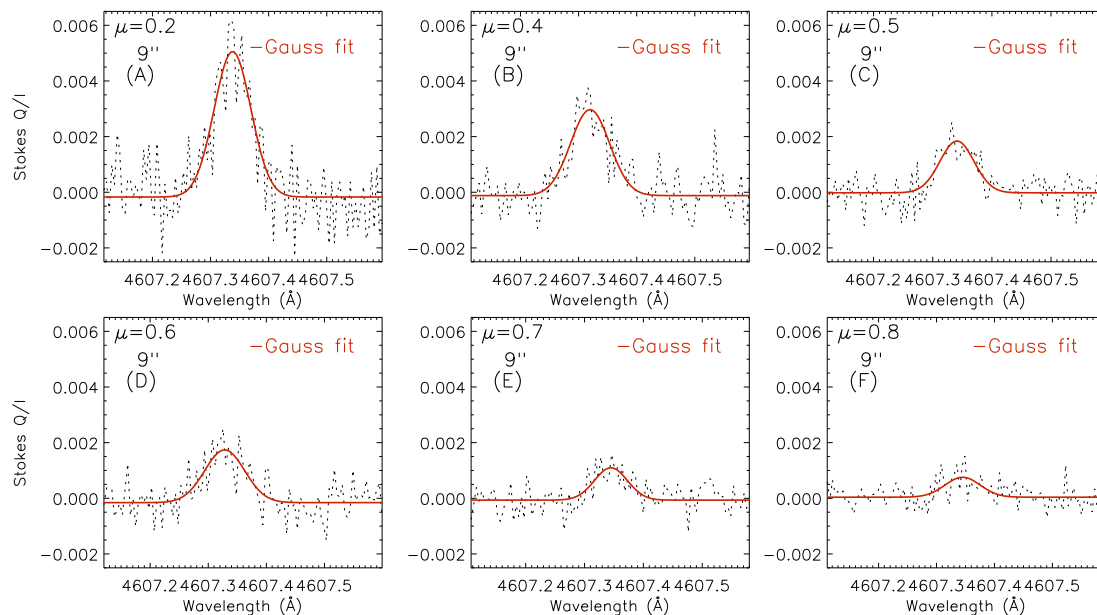


Fig. 4. Q/I profiles obtained at $9''$ spatial position for $\mu = 0.2$ to 0.8 . These profiles correspond to the Stokes Q/I images shown in Fig. 1 (panels A–F). The red lines are the Gaussian fits to the profiles.

the intensity and the Q/I peak amplitudes) is true. As such it is worth noting that having obtained low p -value only serves to discard the null hypothesis, but cannot be taken as confirmation of a positive correlation. The calculated p -values for all the measurements are given in the fourth column of Table 3. For most of the measurements, the obtained p -values are found to be less than 10^{-3} , which corresponds to a confidence level of 99.9% for rejecting the null hypothesis.

Table 3. Obtained Pearson correlation coefficient (r), probability p -value with total number of points (N) from scatter plot at different μ .

Limb distances (μ)	N	r	p -value (approximate)
0.2	328	0.274	4.7×10^{-7}
0.38	280	0.197	9.2×10^{-4}
0.4	980	0.266	6.7×10^{-16}
0.44	280	0.386	1.5×10^{-8}
0.5	420	0.147	2.5×10^{-3}
0.6	280	0.149	1.2×10^{-2}
0.7	280	0.179	2.6×10^{-3}
0.8 e	280	0.237	6.3×10^{-5}

4. Discussion and conclusion

We performed scattering polarization measurements of the $\text{Sr I } 4607.3 \text{ \AA}$ line at different limb distances with ZIMPOL at the GREGOR telescope in Tenerife. The measurements were taken between $\mu = 0.2$ and 0.8 on the solar disk for different time duration depending upon the seeing condition (see Table 1). The direction of positive Stokes Q was always parallel to the nearest solar limb. We averaged a few subsequent frames over time for all the measurement to improve the S/N in the Stokes images. The number of frames averaged (total integration time) at each μ are different (see Table 2), depending upon the signal obtained at that position. We find spatial variations of the Q/I scat-

tering polarization signal of the $\text{Sr I } 4607 \text{ \AA}$ line at all measured positions. These obtained spatial variations of the Q/I scattering polarization signal are not directly comparable among all μ . These results were obtained with a spatial resolution between $\sim 0.66''$ and $0.99''$. The spatial scale of the observed variations is comparable to the granular scale. We find a positive correlation between the scattering polarization peak amplitudes of the $\text{Sr I } 4607 \text{ \AA}$ line and the continuum intensity at every measured position (as shown in Table 3). This implies, statistically, that the polarization inside granular regions is higher than in the intergranular lanes. The positive correlation obtained in this work supports the results reported independently by Malherbe et al. (2007) and Bianda et al. (2018), obtained in both cases at $\mu = 0.3$ using a spectrograph.

The positive correlation found here seemingly contradicts the negative correlation reported by Zeuner et al. (2018), obtained at $\mu = 0.6$ with a spatial resolution of 0.16 pixel^{-1} and spectral resolution 25 m\AA with the FSP mounted on filter-graph TESOS at the VTT in Tenerife. They acquired two dimensional Stokes images (FOV $20'' \times 20''$) with 2.5 s integration time per wavelength position, and the noise in the linear Stokes is 0.3% . In our measurement, the acquired Stokes Q/I image has a noise level of 0.22% for a total integration time of 2.9 min with a spatial resolution of $\sim 0.66'' \text{ pixel}^{-1}$ and spectral resolution 10 m\AA . The correlation coefficient obtained by Zeuner et al. (2018) is $r = -0.17$ at $\mu = 0.6$, while our obtained result is $r = +0.15$ at the same position. Their observation supports the simulation by del Pino Alemán et al. (2018), that foresees an anti-correlation when assuming a high spatial resolution ($0.1''$). By numerically deteriorating the S/N and the spectral and spatial resolutions of the simulated observations, del Pino Alemán et al. (2018) showed that it is possible to reproduce the positive correlation. Their theoretical study also suggests that, for investigating the scattering polarization signals of the $\text{Sr I } 4607 \text{ \AA}$ line, a better instrument would be a 2D spectropolarimeter with a spectral resolution not worse than 20 m\AA , a spatial resolution $\sim 0.1''$ and a polarimetric sensitivity better than 10^{-4} . In our measurement, the spectral resolution is better than the setup used by

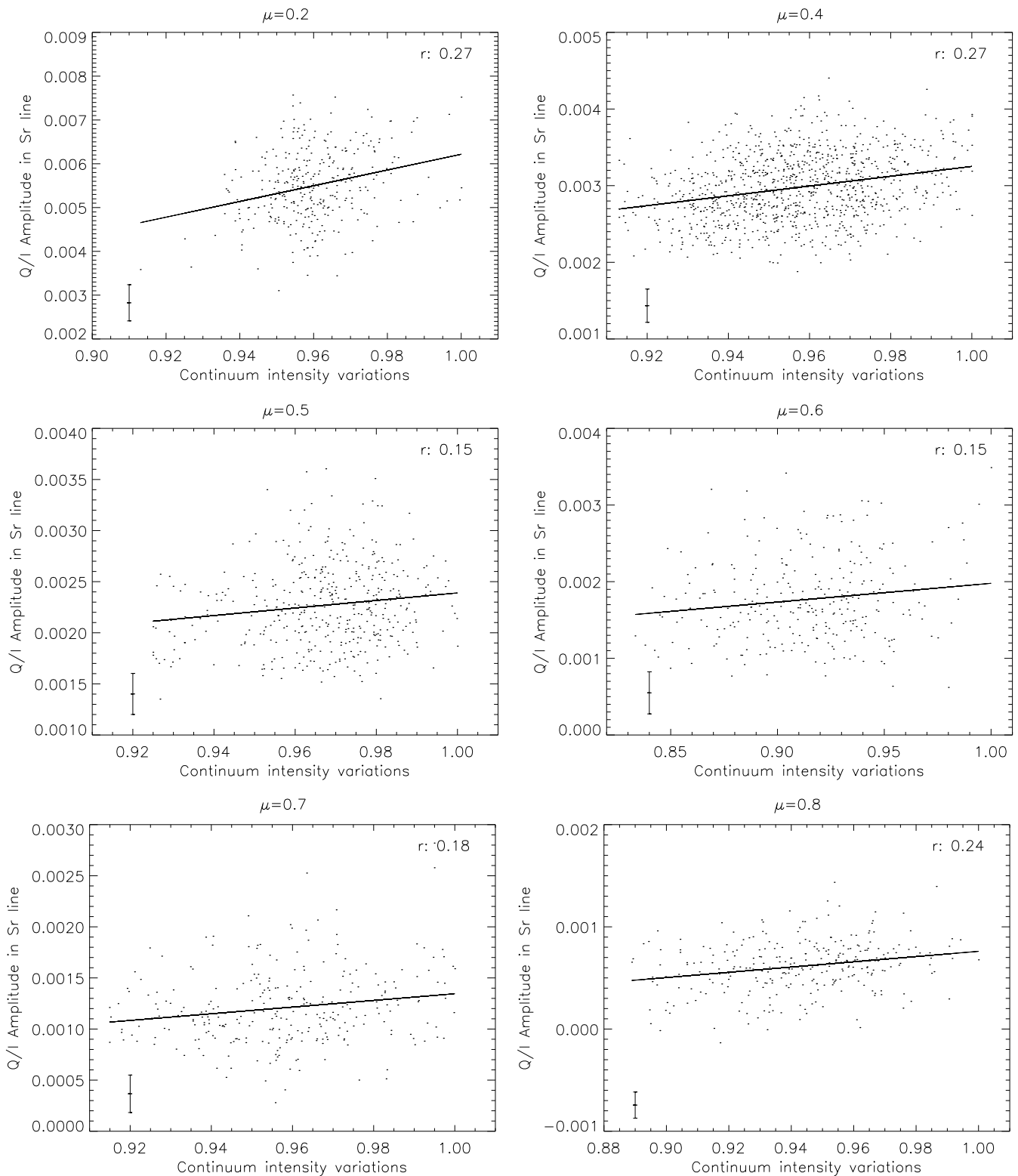


Fig. 5. Scatter plot relating amplitudes of Sr I 4607 Å Q/I peak to normalized continuum intensity at different μ . The solid line represents a linear regression of the data. Its positive slope indicates larger polarization in the granulation. The Pearson correlation coefficient (r) value is annotated in each graph. The estimated error at all points is given by the error bar in the bottom left corner of each plot.

Zeuner et al. (2018), although the spatial resolution is poor. We attribute the difference between the sign of the correlation found by us and the one reported by Zeuner et al. (2018) to the lower spatial resolution, longer integration time, and different S/N of our observations.

The observed results presented here are mostly limited by seeing conditions and by the available photon statistics. A significant improvement of this study can be achieved by performing imaging polarimetric measurements at the line core of the Sr I line with high spatial resolution in a large telescope such

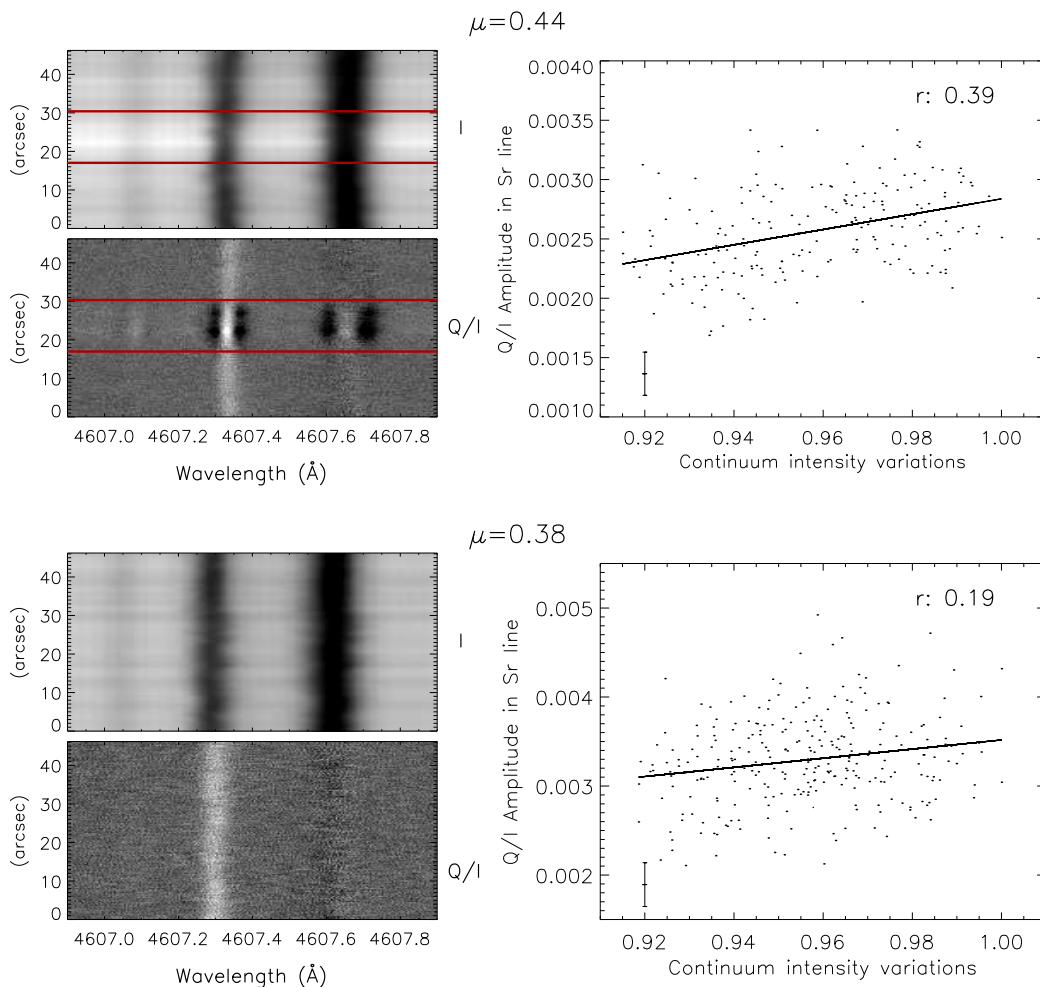


Fig. 6. Left: Averaged Stokes images (I and Q/I) at $\mu=0.44$ (upper panel) and 0.38 (lower panel). Right: Scatter plots relating amplitudes of Q/I peak signals to continuum intensity. The Pearson correlation coefficients (r) are reported in the scatter plots. In the measurements taken at $\mu = 0.44$, the active region is excluded for the calculation of r . Two red horizontal lines show the excluded spatial portion in the top left Stokes I and Q images. The estimated error for each point is shown in the bottom left of each plot.

as Daniel K. Inouye Solar Telescope. In the future we intend to develop a Fabry-Perot filter-based polarimeter system for conducting synoptic measurements of the Sr I 4607 Å line, with the goal of investigating the subgranular photospheric magnetic field. This system could be installed as a second generation instrument on Daniel K. Inouye Solar Telescope.

Acknowledgements. IRSOL is supported by the Swiss Confederation (SEFRI), Canton Ticino, the city of Locarno and the local municipalities. This research work was financed by SNF 200020_169418. The 1.5-meter GREGOR solar telescope was built by a German consortium under the leadership of the Kiepenheuer-Institut für Sonnenphysik in Freiburg with the Leibniz-Institut für Astrophysik Potsdam, the Institut für Astrophysik Göttingen, and the Max-Planck-Institut für Sonnensystem forschung in Göttingen as partners, and with contributions by the Instituto de Astrofísica de Canarias and the Astronomical Institute of the Academy of Sciences of the Czech Republic. We thank the referee for insightful comments which helped us to improve the content in the manuscript.

References

- Berkefeld, T., Schmidt, D., Soltau, D., Heidecke, F., & Fischer, A. 2016, in Proc. SPIE, Vol. 9909, Adaptive Optics Systems V, 990924
- Bianda, M., Berdyugina, S., Gisler, D., et al. 2018, A&A, 614, A89
- del Pino Alemán, T., Trujillo Bueno, J., Štěpán, J., & Shchukina, N. 2018, ApJ, 863, 164
- Faurobert, M., Arnaud, J., Vigneau, J., & Frisch, H. 2001, A&A, 378, 627
- Faurobert-Scholl, M. 1993, A&A, 268, 765
- Feller, A., Iglesias, F. A., Nagaraju, K., Solanki, S. K., & Ihle, S. 2014, in Astronomical Society of the Pacific Conference Series, Vol. 489, Solar Polarization 7, ed. K. N. Nagendra, J. O. Stenflo, Q. Qu, & M. Samooprna, 271
- Gandorfer, A. 2002, The Second Solar Spectrum: A high spectral resolution polarimetric survey of scattering polarization at the solar limb in graphical representation. Volume II: 3910 Å to 4630 Å
- Gisler, D. 2005, Phd thesis, ETH-Zurich
- Hofmann, A., Arlt, K., Balthasar, H., et al. 2012, Astronomische Nachrichten, 333, 854
- Iglesias, F. A., Feller, A., Nagaraju, K., & Solanki, S. K. 2016, A&A, 590, A89
- Malherbe, J.-M., Moity, J., Arnaud, J., & Roudier, T. 2007, A&A, 462, 753
- Ramelli, R., Balemi, S., Bianda, M., et al. 2010, in Proc. SPIE, Vol. 7735, Ground-based and Airborne Instrumentation for Astronomy III, 77351Y
- Ramelli, R., Gisler, D., Bianda, M., et al. 2014, in Proc. SPIE, Vol. 9147, Ground-based and Airborne Instrumentation for Astronomy V, 91473G
- Schmidt, W., von der Lühe, O., Volkmer, R., et al. 2012, in Astronomical Society of the Pacific Conference Series, Vol. 463, Second ATST-EAST Meeting: Magnetic Fields from the Photosphere to the Corona., ed. T. R. Rimmele, A. Tritschler, F. Wöger, M. Collados Vera, H. Socas-Navarro, R. Schlichenmaier, M. Carlsson, T. Berger, A. Cadavid, P. R. Gilbert, P. R. Goode, & M. Knölker, 365
- Soltau, D. 1981, in Solar instrumentation: What's next?, ed. R. B. Dunn, 600
- Stenflo, J. O., Bianda, M., Keller, C. U., & Solanki, S. K. 1997, A&A, 322, 985
- Trujillo Bueno, J. & Shchukina, N. 2007, ApJ, 664, L135
- Trujillo Bueno, J., Shchukina, N., & Asensio Ramos, A. 2004, Nature, 430, 326
- Zeuner, F., Feller, A., Iglesias, F. A., & Solanki, S. K. 2018, A&A, 619, A179